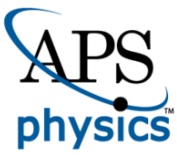

Electron-impact dissociative excitation cross sections for singlet states of molecular hydrogen

Jonathan K. Tapley, Liam H. Scarlett, Jeremy S. Savage, Dmitry V. Fursa, Mark C. Zammit, and Igor Bray

Phys. Rev. A **98**, 032701 — Published 4 September 2018

DOI: 10.1103/PhysRevA.98.032701

Electron-impact dissociative excitation cross sections for singlet states of molecular hydrogen

Jonathan K. Tapley[1], Liam H. Scarlett[1],* Jeremy S. Savage[1], Dmitry V. Fursa[1], Mark C. Zammit[2], and Igor Bray[1]
[1] *Curtin Institute for Computation and Department of Physics, Astronomy and Medical Radiation Sciences, Curtin University, Perth, Western Australia 6102, Australia and*
[2] *Theoretical Division, Los Alamos National Laboratory, Los Alamos, New Mexico 87545, USA*
(Dated: July 27, 2018)

We report cross sections for electron-impact dissociative excitation of the $B\ ^1\Sigma_u^+$, $C\ ^1\Pi_u$, $D\ ^1\Pi_u$, $B'\ ^1\Sigma_u^+$ and $E,F\ ^1\Sigma_g^+$ singlet states of molecular hydrogen from all $v_i = 0$–14 vibrational levels of the ground $X\ ^1\Sigma_g^+$ state. Calculations are performed using the adiabatic-nuclei convergent close-coupling method formulated in prolate spheroidal coordinates from threshold to 500 eV. Agreement with previous calculations varies with transition and impact energy, ranging from excellent to poor. Agreement with available experiment is generally good.

I. INTRODUCTION

Electron-impact dissociative excitation (DE) of molecular hydrogen (H_2) is a dominant process in governing the kinetics of fusion, atmospheric, and interstellar plasmas. It is a significant mechanism for molecular break-up in the interstellar medium [1, 2], and a contributing factor to the hot atomic hydrogen plume observed in the Saturnian atmosphere [3, 4]. Furthermore, DE is a fundamental process in collisional-radiative models [5], and the production of energetic atomic hydrogen [6] in fusion plasmas.

Electron-impact DE in H_2 occurs via excitations to both the singlet and triplet vibrational continua, and is schematically represented as

$$\begin{aligned} \mathrm{H}_2(X\ ^1\Sigma_g^+, v_i) + e^- \rightarrow\ & \mathrm{H}_2(f, \varepsilon_f) + e^- \\ & \downarrow \\ & [\mathrm{H}(n,\ell) + \mathrm{H}(n',\ell')]\,(\varepsilon_f) + e^-, \end{aligned} \tag{1}$$

where v_i denotes the initial vibrational level, and ε_f is the final vibrational continuum state energy in the excited electronic state f.

There have been only a few calculations of DE cross sections, with the majority of studies focusing on scattering from the ground vibrational level (for details see Ref. [7]). Cross sections for the production of H($1s$) and H($2s$) atoms via excitation of the $B'\ ^1\Sigma_u^+$, $E,F\ ^1\Sigma_g^+$, and $e\ ^3\Sigma_u^+$ states were calculated by Chung et al. [8] using the Born-Rudge and Born-Ochkur theories, Mu-Tao et al. [9] using the distorted wave approximation, and by Liu and Hagstrom [10] using the Bethe approximation. The first Born approximation has been applied by Borges et al. [11] at high impact energies (E_i = 100–1000 eV) for DE of the $B\ ^1\Sigma_u^+$ and $C\ ^1\Pi_u$ states (leading to the production of H($1s$) and H($2p$) atoms) and the $B'\ ^1\Sigma_u^+$ state (producing H($1s$) and H($2s$)). Additionally, Celiberto et al. [12] calculated cross sections describing DE to several low lying singlet states and the $b\ ^3\Sigma_u^+$ state using the impact-parameter method for scattering on all vibrational levels of the ground electronic state. It should be noted that these theories are predominantly based on generalized Born and Bethe approximations, or are semi-classical in formulation, and hence are not expected to produce accurate results at low to intermediate energies. More recently, thermally averaged DE cross sections for the singlet ungerade continua have been estimated by Liu et al. [13] using a modified Born approximation with input from experiment for excitation functions, for incident electron energies from threshold to 1000 eV. Overall, the previous calculations [8–13] are in broad agreement at high incident energies, however they differ significantly from threshold to intermediate energies with discrepancies of up to a factor of three for some transitions.

Measured DE cross sections can be inferred from H(n,ℓ) production via electron impact excitation, as has been conducted in Refs. [14–16]. However, production of such fragments is not limited to the DE process; predissociation, radiative cascades from higher states, and autoionization all contribute to the yield of atomic hydrogen. These processes must be included in theoretical calculations, making accurate comparison with measurements of H(n,ℓ) production difficult [11]. However, low-energy DE measurements have also been inferred from time-of-flight and electron energy-loss measurements for DE via the repulsive $b\ ^3\Sigma_u^+$ state (producing two H($1s$) atoms) [17–19]. Recently, a joint theoretical and experimental study [20] set a new benchmark for this cross section which is a factor of two lower than the previously recommended cross sections of Yoon et al. [7].

Scarlett et al. [21] presented cross sections for electron-impact dissociation of the ground (electronic and vibrational) state of molecular hydrogen into neutral atomic hydrogen fragments. These results were obtained using the existing convergent close-coupling (CCC) fixed-nuclei (FN) calculations of Zammit et al. [22, 23] together with dissociation fractions obtained using the adiabatic-nuclei (AN) CCC method [24–29], accounting for DE, predissociation (PD), and excitation radiative decay dissociation

*Electronic address: liam.scarlett@postgrad.curtin.edu.au

(ERDD). It was shown that excitation to the repulsive $b\ ^3\Sigma_u^+$ state and the remaining electronic triplet states (either via DE or subsequent radiative cascades to the $b\ ^3\Sigma_u^+$ state) is the dominant dissociation channel at low to intermediate energies ($E_i < 30$ eV), while the corresponding dissociative processes in the singlet system become dominant at intermediate to high energies.

A detailed analysis of the DE processes via excitation of the singlet vibrational continua in H_2 is the focus of this work. We apply the AN CCC method to model electron-impact DE of H_2 via excitation of the $B\ ^1\Sigma_u^+$, $C\ ^1\Pi_u$, $B'\ ^1\Sigma_u^+$, $D\ ^1\Pi_u$, and $E, F\ ^1\Sigma_g^+$ states from all bound vibrational levels of the $X\ ^1\Sigma_g^+$ state.

We compare the CCC DE results with the previous DE calculations from Refs. [8, 9, 11–13]. For the $B'\ ^1\Sigma_u^+$ state we also compare with experimental estimates of the DE cross section inferred by Borges et al. [11] from the measurements of H($2s$) production by Vroom and de Heer [14], Möhlmann et al. [15], and Ajello et al. [16]. A detailed comparison with measurements of the production of specific neutral atomic fragments will be deferred to future work in which other dissociation channels will be considered. Unless specified otherwise, atomic units are used throughout the paper.

II. THEORY

In this section we briefly discuss the molecular CCC method and the relevant formulas for calculation of DE cross sections. Refer to Refs. [26, 27] for more detailed discussions.

A. Fixed-nuclei molecular CCC method

The theory is formulated in prolate spheroidal coordinates for the body-frame of reference, with the two focal points coincident with the positions of the nuclei. The Born-Oppenheimer approximation is applied to the total scattering wave function, reducing the close-coupling problem to one involving only electronic degrees of freedom at each internuclear distance R. The fixed-nuclei approximation allows scattering calculations to be performed at a single value of R, usually taken to be either the equilibrium distance or the mean internuclear distance of the ground vibrational state. To account for the vibrational motion we utilize the adiabatic-nuclei approximation, detailed in Sec. II B.

Diagonalization of the electronic H_2 Hamiltonian $H_{\rm T}$ in a basis of anti-symmetrized two-electron configurations [21, 22] results in a set of electronic target pseudostates Φ_n^N satisfying

$$\langle \Phi_{n'}^N | H_{\rm T} | \Phi_n^N \rangle = \epsilon_n^N \delta_{n'n}, \tag{2}$$

where the superscript N denotes the number of target pseudostates and ϵ_n^N is the energy of state Φ_n^N. Here the index n stands for the quantum numbers of orbital angular momentum projection m, parity π, and spin s which characterize the target states. The underlying one-electron basis used in the diagonalization procedure consists of Sturmian (Laguerre) functions. This allows us to represent a number of low-lying target states with sufficient accuracy, and also model the target continuum with a finite expansion. The calculated energies $\epsilon_n^N(R)$ are a rough measure of the accuracy of the target wave functions. In Fig. 1 we compare the present potential-energy curves (PEC) for the electronic states under consideration with accurate calculations available from the literature [30–33]. The optical oscillator strengths (OOS)

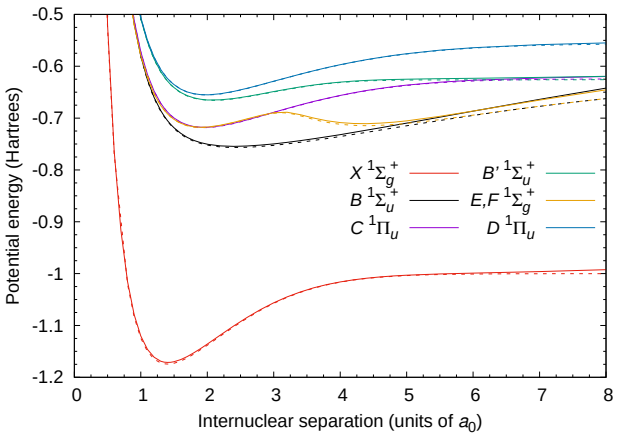

FIG. 1: The present potential-energy curves for several singlet states of H_2 (solid lines), compared with accurate calculations (dashed lines) obtained for the $X\ ^1\Sigma_g^+$ state from Ref. [33], the $B\ ^1\Sigma_u^+$ and $B'\ ^1\Sigma_u^+$ states from Ref. [30], the $C\ ^1\Pi_u$ and $D\ ^1\Pi_u$ states from Ref. [31] and the $E, F\ ^1\Sigma_g^+$ state from Ref. [32].

provide a more sensitive test of the target structure. The length gauge OOS is defined for a given internuclear distance as

$$f_{n,i} = \frac{2g(\epsilon_n^N - \epsilon_i^N)}{3} \left| \langle \Phi_n^N | \hat{\Omega} | \Phi_i^N \rangle \right|^2, \tag{3}$$

where g is the degeneracy factor of the state n. For parallel transitions ($m_n = m_i$) we have $\hat{\Omega} = z$, while for perpendicular transitions ($m_n = m_i \pm 1$) we have $\hat{\Omega} = \mp\frac{1}{\sqrt{2}}(x \pm iy)$. In Fig. 2, the present oscillator strengths are compared with accurate calculations from Refs. [34, 35]. We find the present structure model (OOSs and PECs) is in excellent agreement with previous calculations (within 3%) for the internuclear distances $R = 0.0$–8.0 which span all of the bound vibrational wave functions of the ground electronic state ($v_i = 0$–14).

The total electronic scattering wave function is expanded in terms of its asymptotic channels, leading to a set of momentum-space Lippmann-Schwinger close-

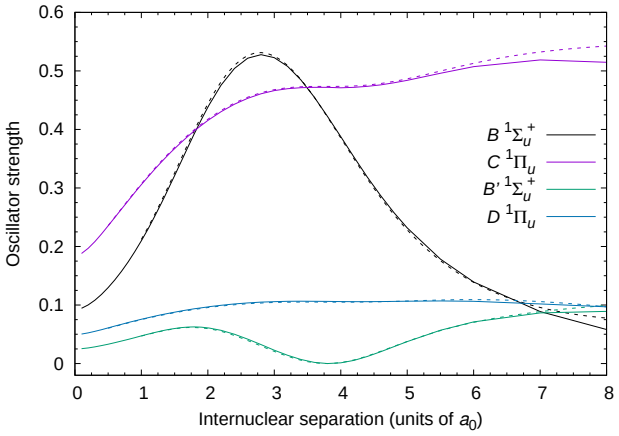

FIG. 2: The present optical oscillator strengths (OOS) for the $X\ ^1\Sigma_g^+$ state to several singlet states of H_2 (solid lines), compared with accurate calculations (dashed lines) obtained from Refs. [34, 35].

coupling equations for the T matrix

$$\langle \boldsymbol{q}_f \Phi_f^N | T^N | \Phi_i^N \boldsymbol{q}_i \rangle \equiv \langle \boldsymbol{q}_f \Phi_f^N | V | \psi_i^{N(+)} \rangle. \tag{4}$$

The projectile plane waves $|\boldsymbol{q}\rangle$ are expanded in spheroidal partial waves (up to $\lambda_{\max}$), allowing the partial-wave T-matrix Lippmann-Schwinger equations

$$T^{M\Pi S}_{f\lambda_f m_f, i\lambda_i m_i}(q_f, q_i; R) = V^{M\Pi S}_{f\lambda_f m_f, i\lambda_i m_i}(q_f, q_i; R) + \sum_{n=1}^{N} \sum_{\lambda, m} \sum\!\!\!\!\!\!\int_q \mathrm{d}q \frac{V^{M\Pi S}_{f\lambda_f m_f, n\lambda m}(q_f, q; R) T^{M\Pi S}_{n\lambda m, i\lambda_i m_i}(q, q_i; R)}{E^{(+)} - \epsilon_k - \epsilon_n^N(R) + i0} \tag{5}$$

to be solved separately for each total symmetry specified by total spin S, parity Π and angular momentum projection M, using standard techniques [27]. The partial-wave orientation-averaged FN integrated cross sections (ICS) for the transition $i \to f$ are obtained using

$$\sigma^{M\Pi S}_{f,i}(E_i; R) = \frac{q_f(R)}{4\pi q_i} \sum_{\substack{\lambda_f, \lambda_i \\ m_f, m_i}} \left| F^{M\Pi S}_{f\lambda_f m_f, i\lambda_i m_i}(E_i; R) \right|^2, \tag{6}$$

where q_f and q_i are the projectile's linear momenta, and the FN partial-wave scattering amplitude is given by

$$F^{M\Pi S}_{f\lambda_f m_f, i\lambda_i m_i}(E_i; R) = -(2\pi)^2 (q_f q_i)^{-1} i^{\lambda_i - \lambda_f} \times T^{M\Pi S}_{f\lambda_f m_f, i\lambda_i m_i}(q_f, q_i; R). \tag{7}$$

Note that in the FN formalism, the outgoing momentum q_f is related to the incident energy E_i and the electronic excitation energy $\epsilon_{f,i} = \epsilon_f - \epsilon_i$ by

$$q_f(R) = \sqrt{2[E_i - \epsilon_{f,i}]}, \tag{8}$$

and so the partial-wave FN scattering amplitude (7) for a given transition is dependent on only E_i and R.

The maximum projectile angular momentum $\lambda_{\max}$ utilized in the solution of Eq. (5) is chosen to yield convergent cross sections with the use of an analytical Born subtraction technique [27]:

$$\sigma^S_{f,i} = \sum_{M\Pi} (\sigma^{M\Pi S}_{f,i} - \tilde{\sigma}^{M\Pi}_{f,i}) + \sigma^{(\mathrm{AB})}_{f,i}, \tag{9}$$

where $\tilde{\sigma}^{M\Pi}_{f,i}$ is the partial-wave Born ICS and $\sigma^{(\mathrm{AB})}_{f,i}$ is the analytic Born ICS. Details of the number of partial waves included in the solution of Eq. (5) are given in Sec. III. The spin averaged cross section is given by

$$\sigma_{f,i} = \sum_S \frac{2S+1}{2(s_i+1)} \sigma^S_{f,i}. \tag{10}$$

For scattering from the ground $X\ ^1\Sigma_g^+$ state of H_2 ($s_i = 0$) considered in this paper, only one total spin channel ($S = 1/2$) is possible.

B. Adiabatic-nuclei method

Following the AN approximation [25, 26, 36], we define the vibrationally resolved electronic excitation (VREE) cross section for the transition $iv_i \to fv_f$

$$\sigma^{\mathrm{PW}}_{fv_f, iv_i} = \frac{q_{fv_f}}{4\pi q_i} \times \sum_{M\Pi S} \frac{2S+1}{2(s_i+1)} \sum_{\substack{\lambda_f, \lambda_i \\ m_f, m_i}} \left| \langle \chi_{fv_f} | F^{M\Pi S}_{f\lambda_f m_f, i\lambda_i m_i}(E_i; R) | \chi_{iv_i} \rangle \right|^2, \tag{11}$$

where the integration is over R, and the outgoing momentum q_{fv_f} is chosen to satisfy energy conservation for the vibrational excitation:

$$\frac{q^2_{fv_f}}{2} + \varepsilon_{fv_f} = \frac{q_i^2}{2} + \varepsilon_{iv_i}. \tag{12}$$

The superscript PW in Eq. (11) indicates that the cross section is a product of the partial-wave calculation only (without the ABS technique which will be introduced for the VREE cross sections below). Note that Eq. (11) differs from the standard AN approximation [36] through the substitution $q_f(R) \to q_{fv_f}$. This substitution partially corrects the violation of energy conservation in the AN approximation at low energies by restoring the correct excitation thresholds. A similar method has been investigated by Mazevet et al. [37] for vibrational excitation $v_i = 0 \to 1, 2$ in low energy e^-–H_2 collisions, for which results are in reasonable agreement with vibrational close-coupling calculations, and in our previous calculations of positron scattering on H_2 [29].

The vibrational wave functions χ_{nv_n} in Eq. (11) satisfy

the radial Schrödinger equation for nuclear motion

$$\left(-\frac{1}{2\mu}\frac{d^2}{dR^2} + \epsilon_n(R) - \varepsilon_{nv_n} \right)\chi_{nv_n}(R) = 0, \qquad (13)$$

where μ is the reduced mass of the molecule, $\epsilon_n(R)$ is the PEC of the electronic state n and ε_{nv_n} is the energy of the vibrational state nv_n. For low rotational quantum numbers, the centrifugal contribution to the nuclear Schrödinger equation is negligible compared to $\epsilon_n(R)$, and hence it has been omitted in Eq. (13). The vibrational wave functions are obtained via a diagonalization procedure using Laguerre basis functions [27]. The basis size is chosen to yield convergent bound states and an adequate discretization of the vibrational continuum.

Obtaining VREE cross sections requires FN collision data calculated at many R points for accurate integration in Eq. (11). To limit the computational resources used for calculations we have utilized a scaling procedure involving two scattering models. The smaller CC(27) model couples only 27 bound states while the larger CCC(210) model couples 210 states, including ionization channels. The number of coupled states included in both models for each target symmetry, as well as the number of negative and positive energy states (relative to the H_2^+ ground state) are summarized in Table I.

TABLE I: Total number of target states in the CC(27) and CCC(210) models for each target symmetry (m, π, s). The number of negative- and positive-energy states relative to the H_2^+ ground state are also shown for $R = 1.448$.

Symmetry	CC(27)	CCC(210)
$^1\Sigma_g$	4	17
$^1\Sigma_u$	2	15
$^3\Sigma_g$	3	15
$^3\Sigma_u$	2	15
$^1\Pi_g$	2	16
$^1\Pi_u$	4	28
$^3\Pi_g$	2	16
$^3\Pi_u$	4	30
$^1\Delta_g$	2	16
$^1\Delta_u$	0	14
$^3\Delta_g$	2	14
$^3\Delta_u$	0	14
$\epsilon < 0$	27	56
$\epsilon > 0$	0	154

In our previous calculations of AN cross sections summed over final vibrational levels, we found that scaling the CC(27) R-dependent ICS, calculated on a fine R grid, to fit CCC(210) calculations performed at only a few R points provided a reliable estimate of the true R-dependent cross sections [26]. Applying a similar procedure to the VREE cross sections (11) utilized in the DE calculation would require the R-dependent scattering amplitudes $F^{M\Pi S}_{f\lambda_f m_f, i\lambda_i m_i}$ to be scaled per partial-wave. Given that the DE cross sections are up to 100 times smaller than their respective total excitation cross sections, we find that the numerical instabilities introduced by scaling each partial-wave amplitude (7), and the subsequent interpolation for integration, can on occasion significantly affect the results. Therefore, we have adopted an alternative approach, expressing the VREE cross section (11) in the following equivalent form:

$$\sigma^{\rm PW}_{fv_f,iv_i} = \frac{q_{fv_f}}{4\pi q_i}\int_0^\infty\int_0^\infty \chi_{fv_f}(R)\chi_{iv_i}(R)\chi_{fv_f}(R')\chi_{iv_i}(R') \times \mathcal{F}_{f,i}(E_i, R, R')\, dR' dR, \qquad (14)$$

where

$$\mathcal{F}_{f,i}(E_i, R, R') = \sum_{M\Pi S}\sum_{\substack{\lambda_f,\lambda_i \\ m_f,m_i}} \frac{2S+1}{2(s_i+1)} \times F^{M\Pi S\ *}_{f\lambda_f m_f, i\lambda_i m_i}(E_i, R) F^{M\Pi S}_{f\lambda_f m_f, i\lambda_i m_i}(E_i, R') \qquad (15)$$

defines a two-dimensional surface with diagonal ($R = R'$) elements proportional to the FN ICS $\sigma_{f,i}(R)$. This surface is scaled from the CC(27) model to fit the CCC(210) model as follows. The ratio $\mathcal{F}^{210}_{f,i}/\mathcal{F}^{27}_{f,i}$ of the CCC(210) surface to the CC(27) surface is calculated at all CCC(210) R points (R=1.448, 2.022, 3.2, 6.0, and 8.0), and then interpolated onto the grid of CC(27) R points (R = 0.4–8.0). The ratio is held constant for $R < 1.448$ to avoid instabilities caused by extrapolation. The scaled CCC-S(210) surface is then obtained by multiplying the CC(27) surface by this ratio function.

To test the accuracy of the scaling procedure, we have conducted CCC(210) calculations over a finer R grid at 40 eV for comparison with the CCC-S(210) results. In Fig. 3, we present the surface $\mathcal{F}_{f,i}(E_i, R, R')$ for the $X\ ^1\Sigma_g^+ \rightarrow B\ ^1\Sigma_u^+$ transition at 40 eV, calculated using the CC(27), CCC(210) and CCC-S(210) models. The qualitative similarities between the CC(27) and CCC(210) results justify the use of the scaling procedure, and we find excellent agreement between the CCC(210) and CCC-S(210) surfaces. Similar agreement was found for all singlet states considered in this paper.

To obtain convergent VREE cross sections with respect to the partial-wave expansion, we implement the ABS procedure (9) within the AN method. This requires the evaluation of the AN analytical and partial-wave Born cross sections.

Performing a partial-wave expansion of the analytical Born transition matrix element

$$\langle \boldsymbol{q}_f \Phi_f | V | \Phi_i \boldsymbol{q}_i \rangle = \sum_{\substack{\lambda\mu \\ \lambda\mu}} i^\lambda V^{\rm (AB)}_{f,i}(Q, R) Y^*_{\lambda\mu}(\hat{\boldsymbol{Q}}), \qquad (16)$$

where $\boldsymbol{Q}$ is the momentum transfer vector and $Y_{\lambda\mu}$ is a

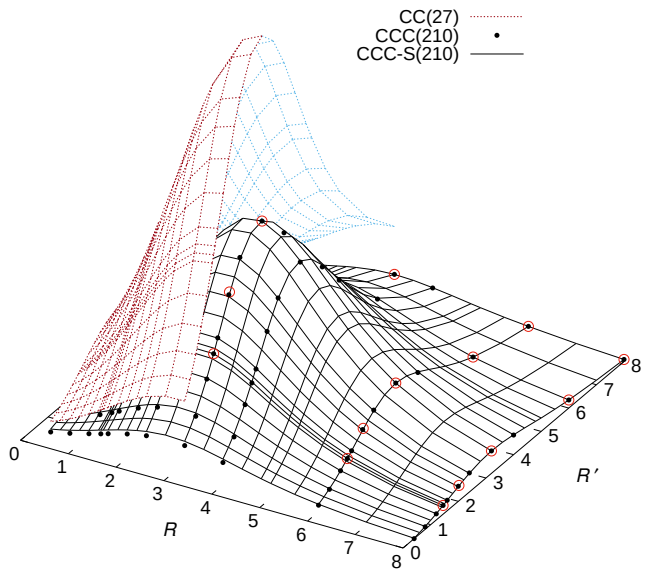

FIG. 3: Comparison of the CC(27), CCC(210) and CCC-S(210) surfaces $\mathcal{F}_{f,i}(E_i, R, R')$ (15) described in the text for the $X\ ^1\Sigma_g^+ \rightarrow B\ ^1\Sigma_u^+$ transition at $E_i = 40$ eV. The upper CC(27) surface is only partially presented for clarity. The open red circles indicate the points at which CCC(210) data was used to produce the scaled CCC-S(210) surface.

spherical harmonic, leads to the analytical Born VREE cross section

$$\sigma^{(\mathrm{AB})}_{fv_f,iv_i} = \frac{q_{fv_f}}{4\pi q_i} \int \sum_{\lambda\mu} \left| \langle \chi_{fv_f} | (2\pi)^2 V^{(\mathrm{AB})}_{\substack{f,i \\ \lambda\mu}}(Q,R) | \chi_{iv_i} \rangle \right|^2 d\Omega. \tag{17}$$

Here, Ω is the scattering solid angle. The scattering angle θ is related to the momentum transfer vector by

$$\theta_{\boldsymbol{Q}} = \arccos\left(\left[q_i - q_f \cos(\theta) \right] / Q \right), \tag{18}$$

where $\theta_{\boldsymbol{Q}}$ is the angle between $\boldsymbol{Q}$ and $\boldsymbol{q}_i$.

The partial-wave Born VREE cross section is obtained by replacing the T-matrix elements in Eq. (7) with the corresponding direct V-matrix elements $\tilde{V}^{M\Pi}_{f,i}$, and substituting the resulting partial-wave scattering amplitudes into Eq. (11), giving

$$\tilde{\sigma}^{\mathrm{PW}}_{fv_f,iv_i} = \frac{q_{fv_f}}{4\pi q_i} \times \sum_{M\Pi} \sum_{\substack{\lambda_f,\lambda_i \\ m_f,m_i}} \left| \langle \chi_{fv_f} | \frac{(2\pi)^2}{q_f q_i} \tilde{V}^{M\Pi}_{f\lambda_f m_f, i\lambda_i m_i}(E_i; R) | \chi_{iv_i} \rangle \right|^2. \tag{19}$$

Using the above definitions the ABS procedure (9) for the VREE cross section is expressed as

$$\sigma_{fv_f,iv_i} = \sigma^{\mathrm{PW}}_{fv_f,iv_i} - \tilde{\sigma}^{\mathrm{PW}}_{fv_f,iv_i} + \sigma^{(\mathrm{AB})}_{fv_f,iv_i}. \tag{20}$$

The DE cross section is then found by summing the VREE cross sections for transitions to vibrational continuum states:

$$\sigma^{\mathrm{DE}}_{f,iv_i} = \sum_{\varepsilon_{fv_f} > D_f} \sigma_{fv_f,iv_i}, \tag{21}$$

where D_f is the Born-Oppenheimer dissociation limit of the electronic state f.

III. RESULTS

We present DE cross sections from threshold to 500 eV for e^-–$H_2(X\ ^1\Sigma_g^+, v_i = 0\text{–}14)$ scattering calculated using both the CC(27) and CCC-S(210) models. The two models both use the same description of the target wave functions. The one-electron functions used to construct the two-electron configurations (see Eqs. (3)–(5) in Ref. [26]) were generated using a basis of $N_\ell = 12 - \ell$ Laguerre functions, up to $\ell_{\max} = 3$. The $1s\sigma_g$ one-electron orbital was generated using a basis of $N_\ell = 60 - \ell$ functions up to $\ell_{\max} = 8$. The scattering calculations in both models were performed using a projectile partial-wave expansion up to $\lambda_{\max} = 6$ at low energies (up to 20 eV) and $\lambda_{\max} = 10$ at higher energies, including all channels of positive and negative parity Π, spin $S = 1/2$ and angular momentum projection M up to $M_{\max} = \lambda_{\max}$. The contribution from higher partial waves was taken into account using the ABS technique (20). For the optically allowed transitions, the partial-wave contribution to the VREE cross sections decreases with increasing incident energy, while the analytical Born contribution increases. For example, below 40 eV the close-coupling term in Eq. (20) makes up approximately 100% of the cross sections for the *ungerade* states we have considered, but this contribution decreases to about 50% by 120 eV on average, and above 300 eV the cross section is dominated by the analytical Born component. For the $X\ ^1\Sigma_g^+ \rightarrow E, F\ ^1\Sigma_g^+$ transition the Born contribution is negligible even at high incident energies.

A. Dissociative excitation from $X\ ^1\Sigma_g^+(v_i = 0)$

In this section we present the DE cross sections for transitions from the $X\ ^1\Sigma_g^+(v_i = 0)$ state to several singlet states, calculated using the CC(27) and CCC-S(210) models, and compare with the available previous calculations. For all states we find qualitative similarities between the CC(27) and CCC-S(210) models, with the smaller model yielding a significantly larger cross section at intermediate energies. This is expected, as the lack of ionization channels in the CC(27) model leads to an overestimation of the discrete electronic excitations. The two models are in better agreement near threshold, where the effect of inter-channel coupling is reduced, and at high energies, where all models converge to the first

Born approximation cross sections.

In Figs. 4–7 results for the $B\ ^1\Sigma_u^+$, $C\ ^1\Pi_u$, $D\ ^1\Pi_u$, and $B'\ ^1\Sigma_u^+$ states are compared with previous calculations [11–13]. The calculations of Celiberto et al. [12] have predicted a peak in the cross sections for each state at energies close to threshold. However, this is not supported by the present CCC calculations or the results of Liu et al. [13]. The DE cross sections of Liu et al. [13] were obtained by experimentally determining a shape function which characterizes the energy dependence of the cross section, and normalizing it to the Born DE cross section at high energies. The error estimates include contributions from the measurement of the shape function as well as the calculation of the Born cross sections. Liu et al. [13] reported that the shape functions for the $B\ ^1\Sigma_u^+$ and $C\ ^1\Pi_u$ states were identical within experimental uncertainties, and utilized this same shape function for the $D\ ^1\Pi_u$ and $B'\ ^1\Sigma_u^+$ states as well. Hence, the resulting DE cross sections for each state have the maximum at the same energy (between 50 and 60 eV). The present results for the $B\ ^1\Sigma_u^+$ state are in excellent agreement with Liu et al. [13] across all energies and converge with Celiberto et al. [12] and Borges et al. [11] at high energies ($E_i > 100$ eV) where the first Born approximation is valid. For the $C\ ^1\Pi_u$ state the CCC results are in good agreement with Liu et al. [13], with small qualitative differences. In fact, for each of the $C\ ^1\Pi_u$, $D\ ^1\Pi_u$, and $B'\ ^1\Sigma_u^+$ states we predict a maximum in the DE cross section at somewhat higher energies than reported by Liu et al. [13].

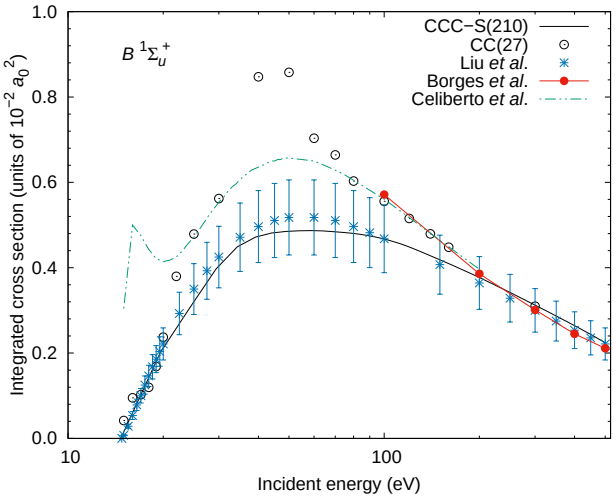

FIG. 4: DE cross sections of the $B\ ^1\Sigma_u^+$ state for scattering from the $X\ ^1\Sigma_g^+(v_i = 0)$ state. The CCC models are discussed in the text and compared with calculations of Borges et al. [11], Celiberto et al. [12] and Liu et al. [13].

The present cross sections for DE of the $D\ ^1\Pi_u$ state (Fig. 6) are in good agreement with Liu et al. [13] up to $E_i = 100$ eV, above which the present results are just underneath the upper limit of the error bars. The $B'\ ^1\Sigma_u^+$ DE cross section is a factor of five larger than the next largest DE cross section (the $C\ ^1\Pi_u$ state). The CCC-

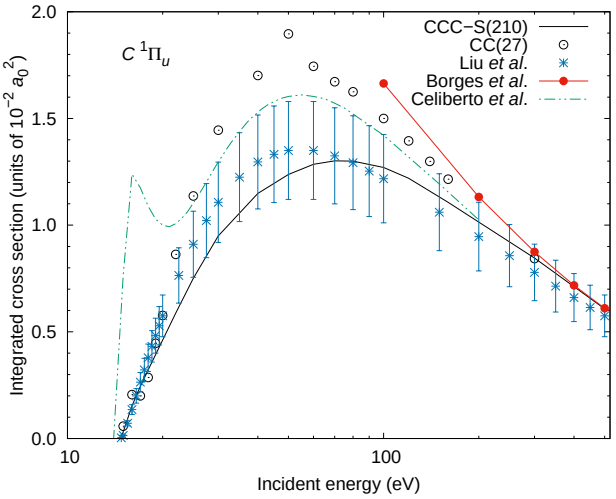

FIG. 5: Same as in Fig. 4 but for the $C\ ^1\Pi_u$ state.

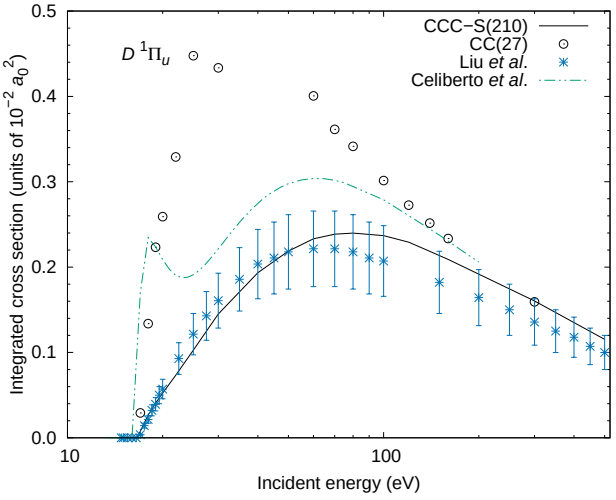

FIG. 6: Same as in Fig. 4 but for the $D\ ^1\Pi_u$ state.

S(210) cross sections for this state are in good agreement with Liu et al. [13] for $E_i < 35$ eV, but for intermediate energies they are about 15% above the quoted error bars. From threshold to 100 eV the CCC results are in significant disagreement with the other theoretical calculations [8, 9, 11, 12], however the CCC results and most of the other theoretical models converge at higher energies. Unlike the other states, the present results for the $B'\ ^1\Sigma_u^+$ state are not within the error bars of Liu et al. [13] at 500 eV. Since channel-coupling effects are negligible in this energy region, the accuracy of the cross section here is determined primarily by the accuracy of the target structure. As demonstrated in Figs. 1 and 2, the present target structure is in excellent agreement with accurate calculations for the range of R points spanned by the ground vibrational wave function, and hence we are confident that the high-energy limit of the present results is correct. Note that the high-energy DE cross sections of

Liu et al. [13] were not obtained by a direct Born calculation, but were instead inferred from photodissociation cross sections calculated using the electric dipole transition moments presented in Refs. [34, 35], and hence it is possible that Liu et al. [13] have somewhat underestimated the $B'\ ^1\Sigma_u^+$ DE cross section at high energies. The discrepancy between the CCC and Liu et al. [13] results for this state at intermediate energies might arise because Liu et al. [13] assume the energy dependence of each cross section to be the same.

Ajello et al. [16] have experimentally estimated the DE contribution via the $B'\ ^1\Sigma_u^+$ state towards H($2s$) production. These data have been used by Borges et al. [11] to partition the H($2s$) production cross sections measured by Möhlmann et al. [15] and Vroom and de Heer [14] in order to determine the contribution from the $B'\ ^1\Sigma_u^+$ state DE, which we have also presented in Fig. 7. We find that the present results are somewhat larger than these estimates. The experiments cited here use Stark quenching for the measurement of H($2s$) production. This process is susceptible to underestimation of the H($2s$) signal resulting from non-radiative processes such as H_3^+ production ($H_2 + H(2s) \rightarrow H_3^+ + e^-$), therefore lowering the estimated DE cross section for the $B'\ ^1\Sigma_u^+$ state [11].

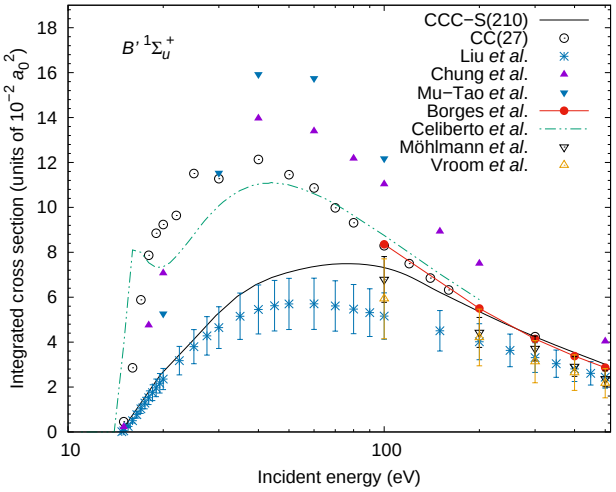

FIG. 7: Same as in Fig. 4 but for the $B'\ ^1\Sigma_u^+$ state. Additional calculations from Chung et al. [8] and Mu-Tao et al. [9] are presented, along with estimates of the $B'\ ^1\Sigma_u^+$ DE cross section obtained by Borges et al. [11] from measurements of H($2s$) production by Vroom and de Heer [14] and Möhlmann et al. [15].

DE cross sections for the optically forbidden $E, F\ ^1\Sigma_g^+$ state transition are presented in Fig. 8 and compared with the previous calculations of Chung et al. [8] and Mu-Tao et al. [9]. At intermediate energies both previous calculations are a factor of 3 and 4 larger than the CCC-S(210) results and remain in disagreement with the CCC results even at high incident energies, $E_i > 100$ eV. The calculations of Chung et al. [8] utilized a single-configuration representation of the target wave functions, which does not provide sufficient accuracy. This introduces substantial errors to the scattering calculations which are present even at high energies. It is also worth mentioning that large inter-channel coupling effects for this transition lead to significant change in shape and absolute values of the total excitation integrated cross section, as observed in the convergence studies of Zammit et al. [22]

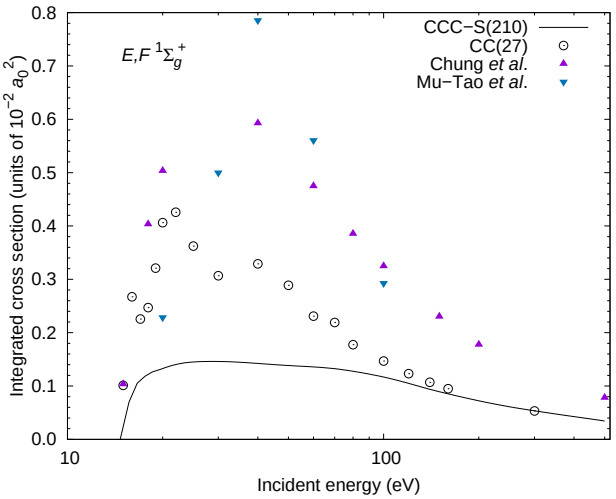

FIG. 8: Same as in Fig. 4 but for the $E, F\ ^1\Sigma_g^+$ state. Comparison with additional calculations by Chung et al. [8] and Mu-Tao et al. [9] is made.

An approximate method for calculating the VREE cross section (11) is to weight the cross section σ_{f,iv_i} for total excitation of the electronic state f from the initial state iv_i with the respective Franck-Condon (FC) factor, giving

$$\sigma_{fv_f,iv_i} \approx \sigma_{f,iv_i} \left| \langle \chi_{fv_f} | \chi_{iv_i} \rangle \right|^2, \tag{22}$$

from which the DE cross section can be obtained using

$$\sigma^{\rm DE}_{f,iv_i} \approx \sigma_{f,iv_i} \left[1 - \sum_{v_f} \left| \langle \chi_{fv_f} | \chi_{iv_i} \rangle \right|^2 \right], \tag{23}$$

where the summation is over the bound vibrational levels of the final electronic state. To test the validity of this approximation, we compare it with the present AN calculations for DE of the $B'\ ^1\Sigma_u^+$ and $C\ ^1\Pi_u$ states from the $v_i = 0$ level of the $X\ ^1\Sigma_g^+$ state in Fig. 9. The FC principle yields a larger DE cross section than the AN calculations (by 20% and 75% at the maximum for the $B'\ ^1\Sigma_u^+$ and $C\ ^1\Pi_u$ states, respectively), although it generally displays the correct qualitative behaviour. The major cause of the discrepancy is that the FC factors in Eq. (22) do not account for the change in the $i \rightarrow f$ transition probability as R varies. This issue is magnified for scattering on excited vibrational states, which span larger regions of the internuclear separation over which

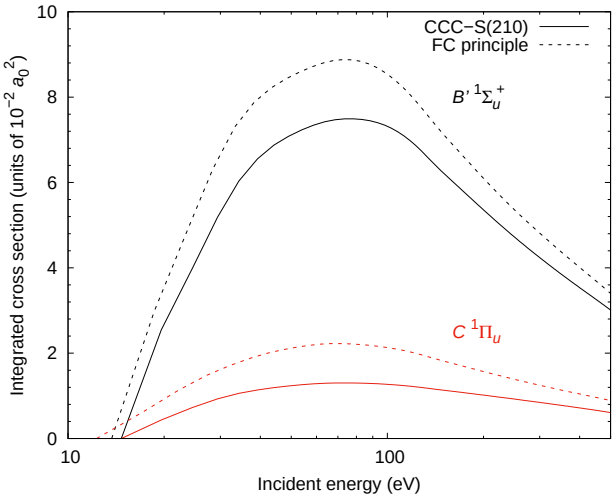

FIG. 9: Comparison of cross sections calculated using the Franck-Condon principle (23) with the present calculations for DE of the $B'\,^1\Sigma_u^+$ and $C\,^1\Pi_u$ states from the $v_i = 0$ level of the $X\,^1\Sigma_g^+$ state.

the excitation probabilities can vary significantly. Hence, for such transitions the full adiabatic-nuclei treatment is required.

B. Dissociative excitation from vibrationally excited levels

In Fig. 10, DE cross sections are presented for scattering on all $X\,^1\Sigma_g^+(v_i = 0\text{–}14)$ vibrational levels. As found in previous studies [12, 13, 26] cross sections for scattering on excited vibrational levels are significantly higher than from the ground state. With increasing v_i the cross sections increase and then decrease nonmonotonically. We represent this behaviour with solid and dashed lines for increasing and decreasing cross sections, respectively. The initial vibrational levels with the largest DE cross sections for excitation of the $B\,^1\Sigma_u^+$, and $C\,^1\Pi_u$, $B'\,^1\Sigma_u^+$, $D\,^1\Pi_u$, and $E, F\,^1\Sigma_g^+$ states are $v_i = 7, 9, 10, 10,$ and 10, respectively. In most cases the largest DE cross section is approximately an order of magnitude larger than the cross section for DE from the $v_i = 0$ level. The notable exception is the $B'\,^1\Sigma_u^+$ state, where the largest DE cross section (for scattering on the $v_i = 10$ level) is only a factor of 2 larger than the $v_i = 0$ cross section.

In Fig. 11, a selection of the CCC DE cross sections are compared with Celiberto et al. [12] for the $B\,^1\Sigma_u^+$, $C\,^1\Pi_u$, $B'\,^1\Sigma_u^+$, and $D\,^1\Pi_u$ states. Although the impact-parameter (IP) results [12] are in significant quantitative disagreement with the present calculation, we note that the qualitative behaviors of the cross sections with respect to both energy and v_i are similar. At high energies, although the present results generally converge to the IP results for low v_i, they are in disagreement for scattering on higher v_i. Note that the accuracy of the target structure utilized by Celiberto et al. [12] was not demonstrated for all internuclear distances spanning the $v_i = 0$–14 vibrational levels. Given the previous success of the molecular CCC method at describing electron collisions with H_2 [22], and the demonstrated accuracy of the present target structure (see Figs. 1 and 2), we believe the CCC-S(210) cross section to be a significant improvement over the previous calculations.

IV. CONCLUSION

We have presented electron-impact DE cross sections for transitions from all $v_i = 0$–14 vibrational levels of the $X\,^1\Sigma_g^+$ state to the $B\,^1\Sigma_u^+$, $C\,^1\Pi_u$, $B'\,^1\Sigma_u^+$, $D\,^1\Pi_u$, and $E, F\,^1\Sigma_g^+$ singlet states. For scattering on the $X\,^1\Sigma_g^+(v_i = 0)$ ground electronic and vibrational state we find good agreement with the previous calculations of Liu et al. [13] for DE through optically allowed transitions. Significant disagreement was found with the previous calculations of Chung et al. [8], Mu-Tao et al. [9], Borges et al. [11], and Celiberto et al. [12] at low and intermediate incident electron energies for all DE cross sections. In the high-energy limit where the first Born approximation is valid we found good agreement with previous calculations for optically allowed transitions but not for the optically forbidden $E, F\,^1\Sigma_g^+$ state. For scattering on excited vibrational levels, previous studies are limited to the IP results of Celiberto et al. [12]. The present results are in qualitative agreement with the IP results in the intermediate and high-energy regions, but significant quantitative disagreement has been found for all transitions. Due to the previous success and demonstrated convergence of the molecular CCC method [20, 22, 25] we expect the present results to be a significant improvement over the previously recommended data. The theoretical techniques utilized in the present work can be extended to produce cross sections for dissociation into specific atomic fragments. Accounting for predissociation and radiative-decay dissociation would allow for comparison with currently available measurements.

V. ACKNOWLEDGMENTS

This work was supported by the United States Air Force Office of Scientific Research, Curtin University, Los Alamos National Laboratory (LANL), and resources provided by the Pawsey Supercomputing Centre, with funding from the Australian Government and Government of Western Australia. L.H.S. acknowledges the contribution of an Australian Government Research Training Program Scholarship, and the support of the Forrest Research Foundation. M.C.Z. would like to specifically acknowledge LANLs ASC PEM Atomic Physics Project for its support. LANL is operated by Los Alamos National Security, LLC for the National Nuclear Security Administration of the U.S. Department of Energy under Contract

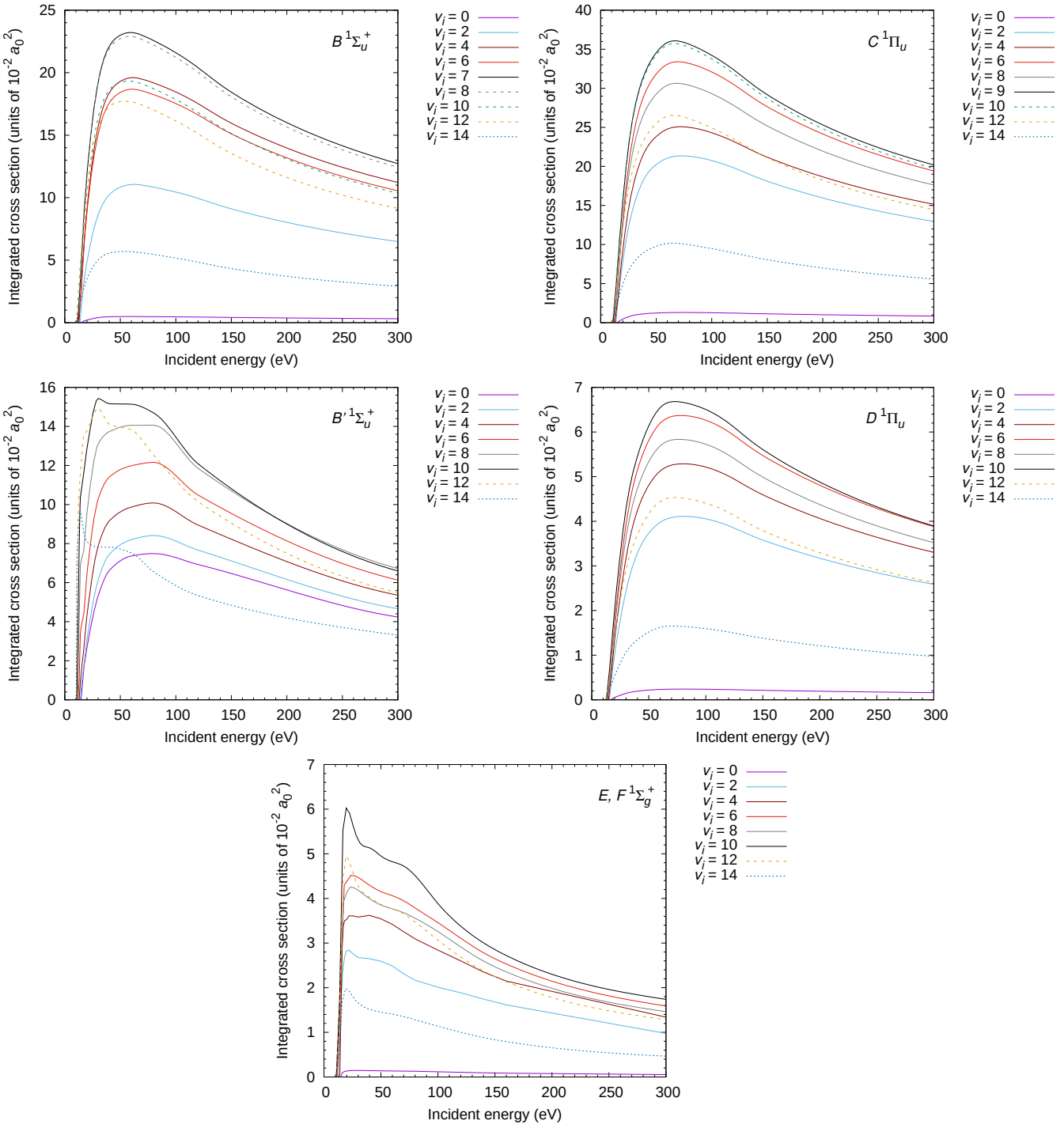

FIG. 10: DE cross sections for the $B\ ^1\Sigma_u^+$, $C\ ^1\Pi_u$, $B'\ ^1\Sigma_u^+$, $D\ ^1\Pi_u$ and $E, F\ ^1\Sigma_g^+$ states for scattering on the $X\ ^1\Sigma_g^+(v_i = 0\text{–}14)$ levels (only even v_i are presented for clarity). Broken lines are used to indicate initial vibrational levels greater than the v_i corresponding to the maximum DE cross section for a given state.

No. DE-AC52-06NA25396.

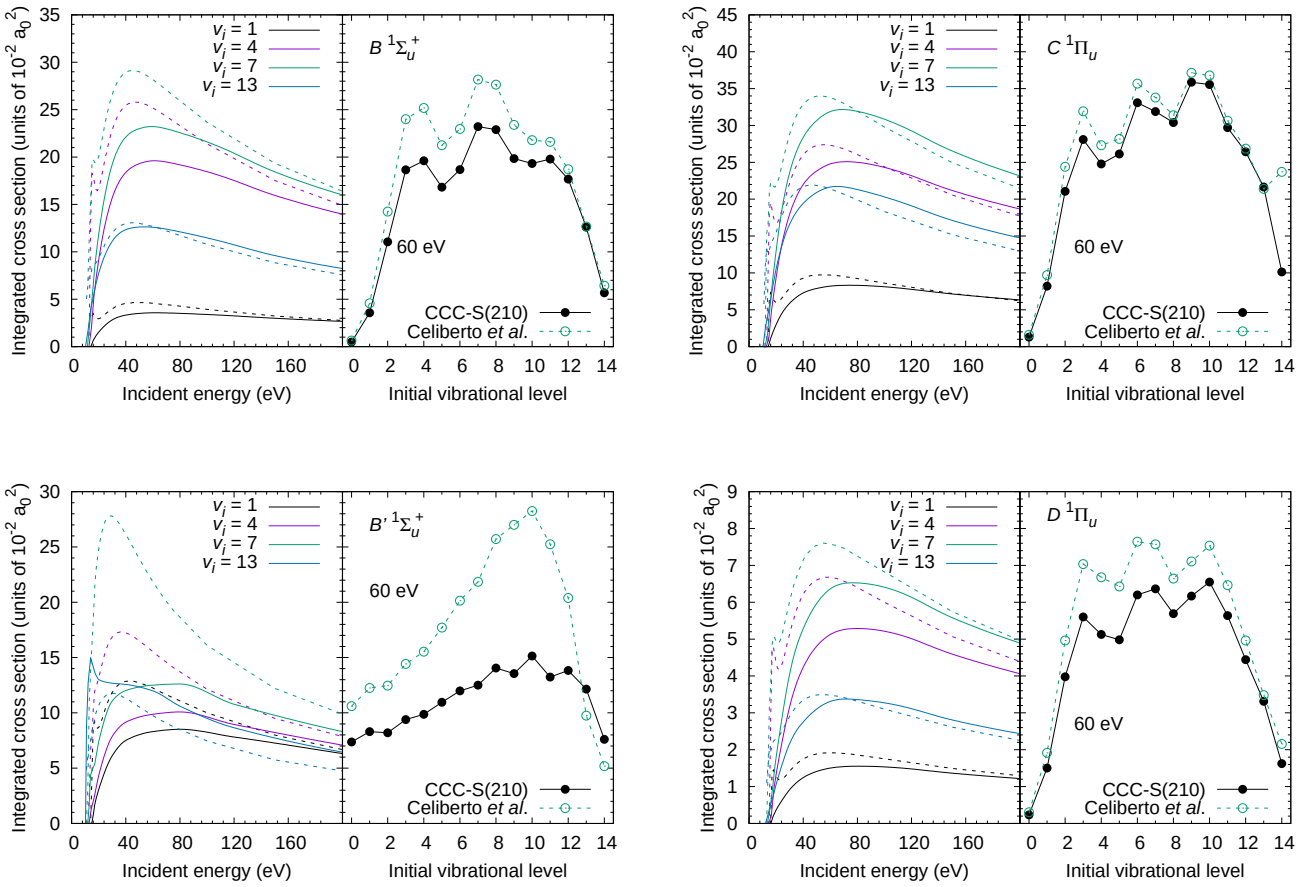

FIG. 11: Comparison of the present DE cross sections (solid lines) with Celiberto et al. [12] (dashed lines) for excitation of the $B\ ^1\Sigma_u^+$, $C\ ^1\Pi_u$, $B'\ ^1\Sigma_u^+$, and $D\ ^1\Pi_u$ states of H_2. The left panel compares the energy dependence of DE cross sections for scattering on various initial vibrational levels v_i, and the right panel displays the dependence of the cross section on v_i for 60 eV incident electrons.

[1] T. Stephens and A. Dalgarno, J. Quant. Spectrosc. Radiat. Transfer **12**, 569 (1972).
[2] H. Abgrall, E. Roueff, X. Liu, and D. E. Shemansky, Astrophys. J. **481**, 557 (1997).
[3] H. Melin, D. E. Shemansky, and X. Liu, Planet. Space Sci. **57**, 1743 (2009).
[4] D. Shemansky, X. Liu, and H. Melin, Planet. Space Sci. **57**, 1659 (2009).
[5] V. A. Shakhatov and Y. A. Lebedev, J. Phys. D **51**, 213001 (2018).
[6] K. Sawada and M. Goto, Atoms **4**, 29 (2016).
[7] J.-S. Yoon, M.-Y. Song, J.-M. Han, S. H. Hwang, W.-S. Chang, B. Lee, and Y. Itikawa, J. Phys. Chem. Ref. Data **37**, 913,931 (200806).
[8] S. Chung, C. C. Lin, and E. T. P. Lee, Phys. Rev. A **12**, 1340 (1975).
[9] L. Mu-Tao, R. R. Lucchese, and V. McKoy, Phys. Rev. A **26**, 3240 (1982).
[10] J. W. Liu and S. Hagstrom, Phys. Rev. A **50**, 3181 (1994).
[11] I. Borges, G. Jalbert, and C. E. Bielschowsky, Phys. Rev. A **57**, 1025 (1998).
[12] R. Celiberto, R. K. Janev, A. Laricchiuta, M. C. ans J. M. Wadehra, and D. E. Atems, At. Data. Nucl. Data Tables **77**, 161 (2001).
[13] X. Liu, D. E. Shemansky, P. V. Johnson, C. P. Malone, M. A. Khakoo, and I. Kanik, J. Phys. B **45**, 15 (2012).
[14] D. A. Vroom and F. J. de Heer, J. Chem. Phys. **50**, 580 (1969).
[15] G. Möhlmann, K. Shima, and F. D. Heer, Chem. Phys. **28**, 331 (1978).
[16] J. M. Ajello, G. K. James, and D. E. Shemansky, Astrophys. J. **371**, 422 (1991).
[17] M. A. Khakoo and J. Segura, J. Phys. B **27**, 2355 (1994).
[18] R. I. Hall and L. Andric, J. Phys. B **17**, 3815 (1984).
[19] H. Nishimura and A. Danjo, J. Phys. Soc. Japan **55**, 3031 (1986).
[20] M. Zawadzki, R. Wright, G. Dolmat, M. F. Martin, L. Hargreaves, D. V. Fursa, M. C. Zammit, L. H. Scarlett, J. K. Tapley, J. S. Savage, et al., Phys. Rev. A **97**, 050702(R) (2018).
[21] L. H. Scarlett, J. K. Tapley, D. V. Fursa, M. C. Zammit, J. S. Savage, and I. Bray, Eur. Phys. J. D **72**, 34 (2018).
[22] M. C. Zammit, J. S. Savage, D. V. Fursa, and I. Bray, Phys. Rev. A **95**, 022708 (2017).
[23] M. C. Zammit, J. S. Savage, D. V. Fursa, and I. Bray, Phys. Rev. Lett. **116**, 233201 (2016).
[24] L. H. Scarlett, M. C. Zammit, D. V. Fursa, and I. Bray, Phys. Rev. A **96**, 022706 (2017).
[25] L. H. Scarlett, J. K. Tapley, D. V. Fursa, M. C. Zammit, J. S. Savage, and I. Bray, Phys. Rev. A **96**, 062708 (2017).
[26] J. K. Tapley, L. H. Scarlett, J. S. Savage, M. C. Zammit, D. V. Fursa, and I. Bray, J. Phys. B: Atom. Molec. Phys. (2018, in press).
[27] M. C. Zammit, D. V. Fursa, J. S. Savage, and I. Bray, J. Phys. B **50**, 123001 (2017).
[28] M. C. Zammit, D. V. Fursa, and I. Bray, Phys. Rev. A **90**, 022711 (2014).
[29] M. C. Zammit, D. V. Fursa, J. S. Savage, I. Bray, L. Chiari, A. Zecca, and M. J. Brunger, Phys. Rev. A **95**, 022707 (2017).
[30] G. Staszewska and L. Wolniewicz, J. Mol. Spectrosc. **212**, 208 (2002).
[31] L. Wolniewicz and G. Staszewska, J. Mol. Spectrosc. **220**, 45 (2003).
[32] T. Orlikowski, G. Staszewska, and L. Wolniewicz, Mol. Phys. **96**, 1445 (1999).
[33] L. Wolniewicz, J. Chem. Phys. **99**, 1851 (1993).
[34] L. Wolniewicz and G. Staszewska, J. Mol. Spectrosc. **217**, 181 (2003).
[35] L. Wolniewicz and G. Staszewska, J. Mol. Spectrosc. **220**, 45 (2003).
[36] N. F. Lane, Rev. Mod. Phys. **52**, 29 (1980).
[37] S. Mazevet, M. A. Morrison, O. Boydstun, and R. K. Nesbet, J. Phys. B **32**, 1269 (1999).